Overview of the Phase Diagram of Ionic Magnetic Colloidal Dispersions

F. Cousin(*), E. Dubois(*), V. Cabuil(*), F. Boué(*), and R.Perzynski(***)

(*) *Laboratoire des Liquides Ioniques et Interfaces Chargées, CNRS UMR 7612, case 63, Université Pierre et Marie Curie, 4, Place Jussieu, 75252 Paris cedex 05, France*

(**) *Laboratoire Léon Brillouin, CEA-CNRS UMR 12, CE-Saclay, 91191 Gif-sur-Yvette, France*

(***) *Laboratoire des Milieux Désordonnés et Hétérogénes, CNRS UMR 7603, case 78, Université Pierre et Marie Curie, 4, Place Jussieu, 75252 Paris cedex 05, France*

Received on 8 January, 2001

We study ionic magnetic colloidal dispersions, which are constituted of γ-Fe_2O_3 nanoparticles dispersed in water, and stabilized with electrostatic interparticle repulsion. The phase diagram ΠV versus Φ (Π: osmotic pressure, V: particle volume, Φ: particle volume fraction) is explored, especially in the range of high Π and high Φ. The osmotic pressure Π of the colloidal dispersion is known either by a measurement either because it is imposed during the sample preparation by osmotic compression. The structure of the colloidal dispersion is determined from Small Angle Neutron Scattering (SANS). Two regimes can be distinguished. At high pressure, fluid and solid phases can exist. Their structure is governed by strong electrostatic repulsion, the range of which is here evaluated. At low pressure, gas, liquid and glassy solids can exist. Their structure results from a sticky hard sphere potential.

I Introduction

Ionic magnetic colloidal dispersions are constituted of nanometric magnetic particles dispersed in water [1-3]. Such dispersions are widely used for technical applications because they are sensitive to a versatile external parameter, the magnetic field. In the present work, the chemically synthesized nanoparticles are constituted of maghemite (γ-Fe_2O_3). They are coated with citrate ligands, which ensure a negative density of charges on the particle surface. The resulting interparticle electrostatic repulsion ensures the stability of the colloidal solution [4].

Such colloidal dispersions can be described as solid spheres suspended in a continuous medium, the solvent. This allows making an analogy between the phase behavior of colloidal dispersions and atomic systems. Although the spatial scales are very different, the interparticle potential has a similar shape in both systems. Therefore, one can expect the same kinds of phases for colloidal dispersions as for atoms: gas (low particle concentration), liquid (large particle concentration), fluid (above a critical point) and solid (amorphous or crystalline dense phase). Indeed, the phase diagram of our colloidal system looks like the phase diagram of atomic systems, with gas-liquid and fluid-solid transitions [5,6]. Such a gas-liquid transition results from a special balance of attractive and repulsive interactions [7], balance which scarcely occurs for electrostatically stabilized colloidal systems, as the one considered and here [8,9]. Moreover, for our magnetic colloids, the existence of this gas-liquid transition also means that the magnetic dipolar interaction has a marginal influence on the interparticle potential in zero magnetic field experiments (as those performed here) [10,11].

Part of the experimental phase diagram of the colloidal dispersion considered here (osmotic pressure Π versus volume fraction Φ) has been previously built up by coupling Small Angle Neutron Scattering (SANS) measurements to determinations of phase separation thresholds [6]. These previous works were dealing with low osmotic pressures and small volume fractions, and with gas-liquid phase transitions. Here we shall explore the borders of the previous diagram, i.e. the range of high osmotic pressures and large volume fractions, using samples prepared by osmotic compression. Our purpose is to study the fluid and solid phases. The comparison of direct measurements of osmotic pressure

to SANS structure factor determinations allows us to give a first characterization of their local structure and to locate them on the $\Pi - \Phi$ diagram with respect to the gas-liquid phase separations.

II Samples and methods

The particles are chemically synthesized in water by coprecipitation of $FeCl_2$ and $FeCl_3$ in an alkaline solution [12]. It leads to γ-Fe_2O_3 particles of density $\rho = 5$ g/cm^3 dispersed in an acidic aqueous medium (pH $\sim$ 2). Their surface is then coated with trisodium citrate molecules, and the pH of the solution is set to 7. The particles surface charge is negative, saturated at a value of 2 charges/nm^2, and neutralized by Na^+ counterions [4]. As the adsorbed citrate ions are in equilibrium with unadsorbed citrate ions, the ionic strength in the solution is due to the concentration $[\text{Cit}]_{\text{free}}$ of these unadsorbed citrate ions and to their sodium counterions.

The volume fraction Φ of the solution is determined from chemical titration of iron [13]. The particle size distribution, assumed to be a lognormal one, is extracted from the magnetization curves measured for low volume fractions ($\Phi < 1\%$) [3]. A two parameter fit of these curves allows determining the mean diameter d_0 ($\ln d_0 =< \ln d >$) and the distribution width σ [3]. The two samples A and B used here have same mean diameter $d_0 = 7$ nm but a different polydispersity index: $\sigma_A = 0.35$ and $\sigma_B = 0.2$. In order to check the good dispersion of the particles at low volume fraction, transmission electron microscopy (see Fig. 1) has been performed on a platinum-carbon replica obtained after a high-pressure freeze fracture (77K and 200 bars) [14].

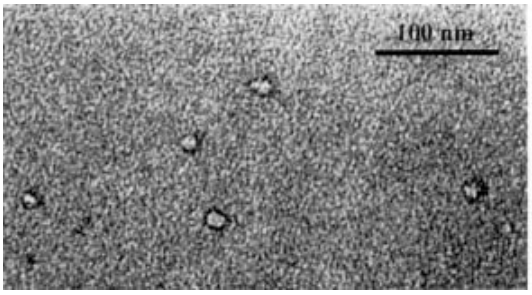

Figure 1. Transmission electron microscopy picture after a freeze fracture under high pressure for sample A with $\Phi = 0.05\%$.

At the end of the chemical synthesis, the citrate concentration $[\text{Cit}]_{\text{free}}$ is at least 5.10^{-2} mol/L, leading to a maximal osmotic pressure of the order of 4000 Pa at $\Phi = 10\%$. Such pressures are measured for $\Phi < 10\%$ with a membrane osmometer (Knauer ref A0330) between 10 Pa and 4000 Pa with an accuracy of 5 Pa [15,16]. The membrane (cellulose 20 kDa) separates two compartments, one filled with the colloidal dispersion and the other filled with a sodium citrate solution, the concentration of which equals $[\text{Cit}]_{\text{free}}$ in the colloidal dispersion.

In order to reach experimentally higher osmotic pressures, the samples are here submitted to an osmotic compression. The colloidal dispersion, placed in a dialysis bag (12-14 kDa), is immerged in a bath solution of known osmotic pressure and known ionic strength. The osmotic pressure is fixed by a polymer (Dextran, $M_W = 110000$ g/mol, Fluka) placed in the reservoir, polymer which fixes the chemical potential of water. The pressure is calibrated and independent of the ionic strength [17]. The ionic strength is imposed by the citrate concentration of the bath solution. The equilibrium is reached in a few weeks. The pressure and the ionic strength of the colloidal magnetic suspension then equal that of the external bath. As the final volume fraction depends on Π and $[\text{Cit}]_{\text{free}}$, it is different from the initial value, and it is determined again after equilibrium.

SANS experiments are performed on the PAXY spectrometer (Orphée reactor, LLB, CEA Saclay, France). Three different configurations of neutron wavelength λ and detector distance Δ ($\lambda = 10$Å, $\Delta = 3.1$ m), ($\lambda = 5$ Å, $\Delta = 1$ m), ($\lambda = 5$ Å, $\Delta = 3.1$ m) were used. It leads to a global range of scattering vectors q between 0.008 Å^{-1} and 0.4 Å^{-1}. The experiments being performed in light water, the measured intensity after subtraction of the incoherent signal is proportional to the nuclear contribution of the particles [18]. In order to determine the form factor of the particles, the scattered intensity of samples A and B is measured for non-interacting dilute particles, i.e. a volume fraction Φ_0 around 1% in the conditions of ionic strength used here. The structure factor $S(q, \Phi)$ of concentrated dispersions is deduced from the detected intensity $I(q, \Phi)$ using: $S(q, \Phi) = (I(q, \Phi)/\Phi)/(I(q, \Phi_0)/\Phi_0)$.

III Results and discussion

Osmotic pressure measurements:

These measurements are performed with the membrane osmometer for sample A at three different citrate concentrations. The results are plotted in Fig. 2 as Π/Φ versus Φ. At low Φ, Π/Φ may be expanded in a virial development

$$\frac{\Pi}{\Phi} = \frac{kT}{V}(1 + \rho^2 N_a V A_2 \Phi + O(\Phi^2)), \qquad (1)$$

where V is the volume of the particle (that we shall assimilate further on to its weight average), ρ is the density of the particle (g/cm^3) N_a is the Avogadro number, and A_2 is the second virial coefficient (mol.g^{-2}.cm^3). If Φ tends toward 0, Π/Φ tends toward kT/V that equals here 30 Pa. In the present experiment:

- Π/Φ increases with Φ which is characteristic of a repulsive regime ($A_2 > 0$).

- Π/Φ versus Φ strongly depends on the citrate concentration.

- the linear development of Π/Φ as a function of Φ given in expression (1) is no longer valid in our experimental range of Φ. Higher order terms have to be taken into account here.

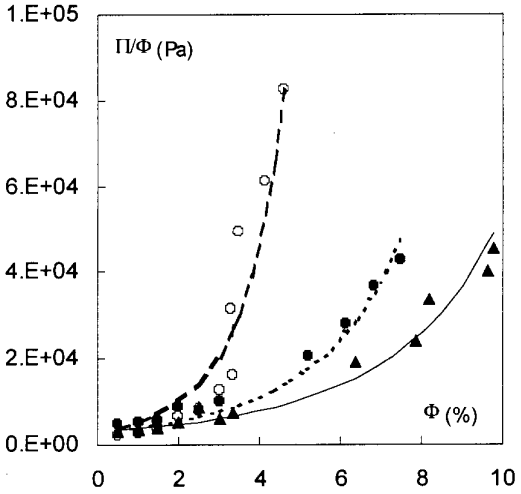

Figure 2. Reduced osmotic pressure Π/Φ as a function of volume fraction Φ for sample A at three different $[\mathrm{Cit}]_{\mathrm{free}}$ values. From top to bottom, $[\mathrm{cit}]_{\mathrm{free}} = 10^{-3}$ mol/L; 5.10^{-3} mol/L; 10^{-2} mol/L. Dashed line, dotted line and full line respectively correspond to best fits of expressions 2 and 3, with δ = 68 Å, 48Å and 38 Å .

Thus other expressions of Π involving higher order terms have to be used to describe the system. Carnahan and Starling have proposed for hard spheres a semi-empirical equation of state that gives the exact virial coefficients until the fourth order [19]:

$$\frac{\Pi}{\Phi} = \frac{kT}{V}\frac{1+\Phi+\Phi^2-\Phi^3}{(1-\Phi)^3}, \qquad (2)$$

In our colloidal dispersions, in the regime explored in Fig. 2, the interaction is repulsive and the system can be considered as constituted of effective hard spheres of diameter $d_0 + 2\delta$, where δ scales as the range of the interparticle interaction. The effective volume fraction Φ_{HS} can be defined by:

$$\Phi_{HS} = \Phi\left(1+\frac{2\delta}{d_0}\right). \qquad (3)$$

The best fits of the Π/Φ data using expressions (2) and (3) are presented in Fig. 2. It gives an evaluation of δ for the three different ionic strengths of the experiment ($[\mathrm{Cit}]_{\mathrm{free}} = 10^{-3}$ mol/L, δ = 68 Å; $[\mathrm{Cit}]_{\mathrm{free}} = 5.10^{-3}$ mol/L, δ = 46 Å; $[\mathrm{Cit}]_{\mathrm{free}} = 10^{-2}$ mol/L, δ = 38 Å). We see that the interaction range δ is $[\mathrm{Cit}]_{\mathrm{free}}$ dependent.

We can compare this interaction range δ to the Debye length that characterizes the range of the interparticle electrostatic repulsion:

$$\kappa_0^{-1} = \left(4\pi l_B \sum_i c_i z_i^2\right)^{-\frac{1}{2}} \qquad (4)$$

l_B being the Bjerrum length (7.2 Å in water at 298 K), c_i and z_i being respectively the concentration and the valency of the ionic species i. Sodium citrate is expected to behave as a 3:1 electrolyte. This leads, for $[\mathrm{Cit}]_{\mathrm{free}} = 5.10^{-3}$ mol/L, to κ_0^{-1} = 18 Å , value much smaller than the experimental value of δ in the same conditions, 46 Å . As a matter of fact, if we suppose now that sodium citrate behaves as a 1:1 electrolyte of same concentration, we obtain κ_0^{-1} = 43.5 Å for $[\mathrm{Cit}]_{\mathrm{free}}$ = 5.10^{-3} mol/L. It is much closer to the experimental value of δ.

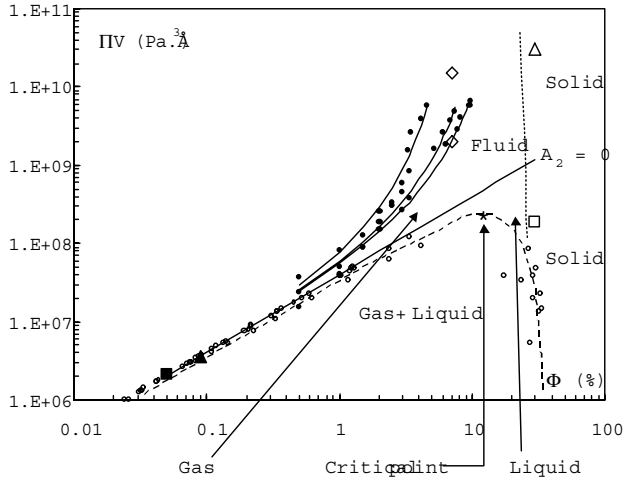

Figure 3. Phase diagram ΠV versus Φ from reference [6]. The open dots correspond to the coexistence lines of the gas-liquid transition and the dashed line is a guide for the eye, showing the location of the critical point. The full dots and full lines correspond respectively to the data and fits from Fig. 2. The straight line corresponds to ΠV for A_2 = 0. The black square corresponds to the conditions of the freeze fracture picture of Fig. 1. The black triangle corresponds to the conditions of coexistence associated to the threshold determinations of Fig. 4. The two open diamonds correspond to the fluid phases from Fig. 5. The open triangle corresponds to the solid phase from Fig. 6 observed at high osmotic pressure. The open square corresponds to the solid phase from Fig. 7 observed at low osmotic pressure. The dotted line is an evaluation of the frontier between solid and fluid phases.

These Π/Φ data and their fits are also reported in Fig. 3 that represents the phase diagram of the colloidal system, as determined in reference [6]. It shows that these osmotic pressure determinations are realized in the monophasic fluid area of the diagram, above the straight line $A_2 = 0$. In this area, $A_2 > 0$, and the repulsive interaction is dominating. Please note that the conditions of the freeze fracture experiment of Fig. 1 (Φ = 0.05% and $\Pi V = 2.110^6$ Pa.Å ^{3}), also reported in Fig. 3, correspond to the same regime. For lower ΠV values, A_2 becomes negative and there is coexistence between gas and liquid phases. The thresholds of the

phase transition (measured using optical microscopy) confirm the special behavior of the citrate electrolyte. The phase separation can be induced by salt addition, here either citrate or sodium chloride, the second being a monovalent electrolyte. Fig. 4 plots the thresholds for sample B at $\Phi = 0.09$ % and $\Pi V = 3.6.10^6$ Pa.Å ^{3}. It shows that citrate addition is nearly equivalent in concentration to NaCl addition to produce the phase separation and thus confirms that sodium citrate behaves here as a 1:1 electrolyte. This could result from finite size effects of citrate ions associated (or not) to counterions condensation.

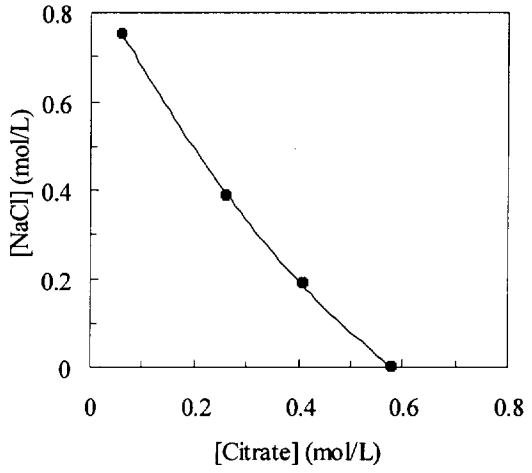

Figure 4. Liquid-gas phase separation induced by addition of NaCl (Sample B, $\Phi = 0.09$ %, $\Pi V = 3.6.10^6$ Pa.Å ^{3}) - Threshold of NaCl concentration as a function of the initial sodium citrate concentration of the solution.

Small Angle Neutron Scattering experiments:

These experiments have been used to explore the area of very *high osmotic pressures* in the phase diagram, area where interparticle repulsion is dominating. This area can only be explored with samples prepared by osmotic compression. Two different kinds of phases can be observed: fluid ones, which flow under gravity, and solid ones, which do not flow under gravity. The structure factor is determined by SANS for two fluid phases (Fig. 5) and one solid phase (Fig. 6). The two fluid phases are made of sample B with the same volume fraction of particles (7%) and two different ionic strengths ($[\mathrm{Cit}]_{\mathrm{free}} = 2.5.10^{-3}$ mol/L and $1.5.10^{-2}$ mol/L, see Fig. 5). The two corresponding structure factors $S(q)$ are very close to each other. Their low value (~0.15) in the very low q limit is characteristic of a strongly repulsive regime.

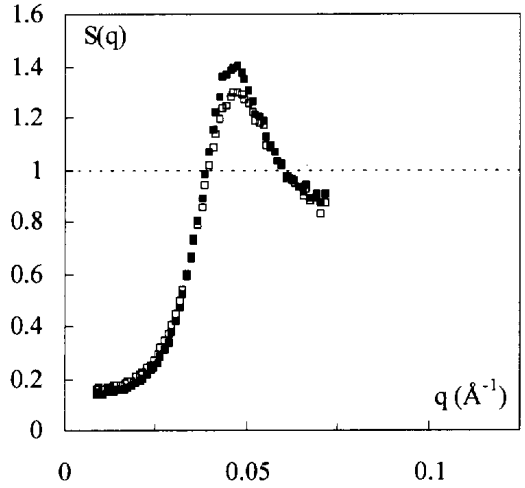

Figure 5. Fluid phases - Structure factor S(q) for sample B at $\Phi = 7\%$ and two citrate concentrations. $[\mathrm{cit}]_{\mathrm{free}} = 2.5\ 10^{-3}$ mol/L (full symbols); $[\mathrm{cit}]_{\mathrm{free}} = 1.5\ 10^{-2}$ mol/L (open symbols).

The solid phase (Fig. 6) is made of sample A with a volume fraction 29.5 % and an ionic strength $[\mathrm{Cit}]_{\mathrm{free}} = 10^{-2}$ mol/L. Its structure factor has the same shape as that of a liquid, and is thus characteristic of a glassy structure. Such a lack of long range order probably results from a too large polydispersity in size of the nanoparticles [8,20].

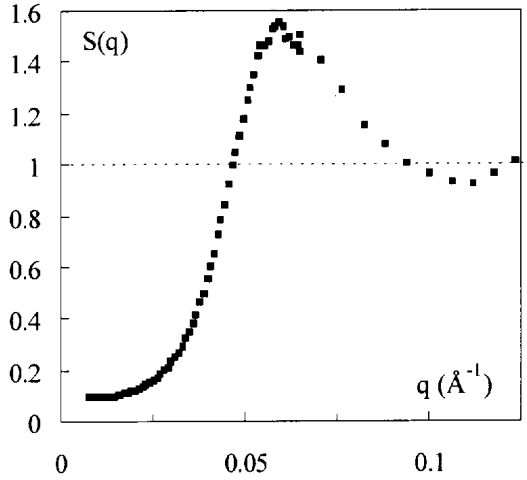

Figure 6. Solid phase at high osmotic pressure ($\Pi = 50000$ Pa) - Structure factor $S(q)$ for sample A at $\Phi = 29.5\%$ and $[\mathrm{cit}]_{\mathrm{free}} = 10^{-2}$ mol/L.

In this high-pressure regime, the distance $d_{q\max} = 2\pi/q_{\max}$, which is associated to the maximum $q_{\max}$ of the structure factor, corresponds to the mean distance d_{mean} between particles in the solution. For example, for the fluid sample with $[\mathrm{Cit}]_{\mathrm{free}} = 2.5.10^{-3}$ mol/L, $d_{q\ \max} = 137$ Å and $d_{\mathrm{mean}} = 136.5$ Å. We also observe that $d_{q\ \max}$ varies as $\Phi^{-1/3}$, like d_{mean}. We conclude that, for such high pressures, the particles are homogeneously dispersed in the sample and the interparticle potential is repulsive at all spatial scales.

At lower osmotic pressures, the phase diagram (Fig. (3)) presents at low volume fraction a gas-liquid transition associated to a critical point [6,15]. In the area of large particle volume fractions, a glassy solid phase, prepared by osmotic compression, is also observed. Fig. 7 presents the structure factor of a solution based on sample B of volume fraction 30% and ionic strength $[\mathrm{Cit}]_{\mathrm{free}} = 1.5$ mol/L. Contrary to the former case, the maximum of the structure factor corresponds here to the contact distance between two particles (taking into account the thickness of the adsorbed citrate layer): $d_{q\max} = 75$ Å and $d_{\mathrm{contact}} = 80$ Å . For such low pressures, the particles are no longer homogeneously dispersed in the sample. Let us also note an upturn of $S(q)$ at low q, characteristic of an interparticle attraction. It results that the interparticle potential is that of sticky hard spheres.

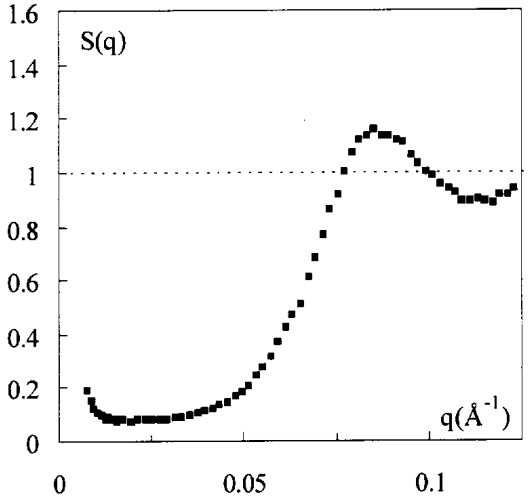

Figure 7. Solid phase at low osmotic pressure ($\Pi = 750$ Pa) - Structure factor $S(q)$ for sample B at $\Phi = 30\%$ and $[\mathrm{cit}]_{\mathrm{free}} = 1.5$ mol/L.

IV Conclusion

We are able to prepare highly concentrated dispersions of magnetic particles of known ionic strength and known osmotic pressure, which allow us to explore large areas at the borders of the phase diagram. Two regimes can be distinguished:

- *at low salinity (high osmotic pressure)*, the system presents fluid phases and solid phases only. Their structure is ruled by the strong electrostatic repulsion, the range of which is here evaluated. It is of the order of the Debye length if it is calculated considering the sodium citrate as an 1:1 electrolyte. The solid phase here obtained has a colloidal glass structure. This has to be related first to the sample polydispersity, and second to the experimental way to prepare the sample that may not allow it to explore all configurations.

- *at high salinity (low osmotic pressure)*, a glassy solid phase is also observed at large particle volume fractions. The structure factor is then modified by an attractive interaction. Within this range, the repulsion is screened, and the attractive part of the interparticle potential can be seen directly on the structure factor. The resulting potential can be described as that of sticky hard spheres.

In that work, we have explored the borders of the phase diagrams towards large pressures and volume fractions as summarized in Fig. 3. Although this gives a good idea of the global phase behavior, several points remain to study in forthcoming works:

- where is exactly the boundary between the fluid and the solid phase ?

- how does the colloid behave in the neighborhood of the critical point ?

- are there a triple point and a coexistence between gas and solid phases at low osmotic pressure ?

- is there a flocculation area in the diagram, for low ionic strengths, when the surface charge density depends on the $[\mathrm{Cit}]_{\mathrm{free}}$ concentration ?

As mentioned in the introduction, the magnetic dipolar interaction has a negligible influence for such experiments without an applied magnetic field. We observe the same kind of phase diagram as with a non-magnetic colloidal dispersion. The next step will be of course the study of the fluid, liquid and solid phases obtained under magnetic field.

Acknowledgments

We thank Delphine Talbot for preparing the initial colloidal dispersions. High-pressure freeze fracture replicas have been done by J.P. Lechaire in Laboratoire de Biologie Marine, Université Paris VI. The corresponding electron microscopy picture has been obtained by M. Lavergne in Centre Régional de Mesures Physiques, Université Paris VI.

References

[1] R. Rosensweig, in *Ferrohydrodynamics* (Cambridge University Press, Cambridge, 1985).

[2] E. Blums, A. Cebers and M.M. Maiorov in *Magnetic fluids*, edited by de Gruyter (New York, 1997).

[3] in *Magnetic fluids and Applications - Handbook*, edited by Berkovsky (Begell House, New York, 1996).

[4] E. Dubois, V. Cabuil, F. Boué, and R. Perzynski, J. Chem. Phys. **111**, 7147 (1999).

[5] F. Cousin and V. Cabuil, Prog. Colloid Polymer Sci. **115**, 77 (2000).

[6] E. Dubois, R. Perzynski, F. Boué and V. Cabuil, Langmuir **13**, 5617 (2000).

[7] C.F. Tejero, A. Daanoun, H.N.W. Lekkerkerker, M. Baus, Phys. Rev. Lett. **73**, 752 (1994).

[8] P.N. Pusey, in Liquids, freezing and glass transitions, edited by J.P. Hansen, D. Levesque, J. Zinn-Justin (North-Holland, Amsterdam, 1991) 765.

[9] J.M. Victor and J.P. Hansen, J. Chem. Soc., Faraday Trans. **2, 81**, 43 (1985).

[10] M.E. van Leeuwen and B. Smit, Phys. Rev. Lett. **71**, 3991 (1993).

[11] M.J. Stevens and G.S. Grest, Phys. Rev. E **51**, 5962 (1995).

[12] R. Massart, IEEE Trans. Mag. MAG-17,1247 (1981); R. Massart, French Patent 79-188-42 (1979); U.S. Patent 4329241 (1982).

[13] G. Charlot, in *Les méthodes de la chimie analytique*, edited by Masson et Cie (Paris, 1966) 737.

[14] D. Fauchadour, T. Pouget, J-P. Lechaire, L. Rouleau and L. Normand, Revue de l'Institut Français du Pétrole, vol **54**(4), 513 (1999).

[15] F. Cousin and V. Cabuil, Journal of molecular liquids, **83** (1-3), 203 (1999).

[16] F. Cousin, Thesis of the University Paris VI, Paris (2000).

[17] C. Bonnet-Gonnet, Thesis of the University Paris VI, Paris (1993).

[18] F. Gazeau, F. Boué, E. Dubois, S. Neveu and R. Perzynski, to be published.

[19] N.F. Carnahan and K.E. Starling, J. Chem. Phys. **51**, 635 (1969).

[20] P. Bartlett, J. Chem. Phys. **107**, 188 (1997).